WARSAW UNIVERSITY OF TECHNOLOGY Index 351733
FACULTY OF CIVIL ENGINEERING
COMMITTEE FOR CIVIL AND WATER ENGINEERING
POLISH ACADEMY OF SCIENCES ISSN 1230-2945

DOI: 10.24425/ace.2024.149879
ARCHIVES OF CIVIL ENGINEERING
Vol. LXX ISSUE 2 2024
pp. 527 –541

Research paper

Parametric optimization scheme of energy dissipation and shock absorption for prefabricated concrete frame

Zhengjian Li[1]

Abstract: The prefabricated concrete frame structure system has advantages such as short construction period and good seismic performance, but its deformation and energy dissipation capacity are poor under earthquake action, making it prone to damage. By improving the analysis and simulation functions of existing finite element analysis for prefabricated structures, the engineering applicability of the analysis algorithm has been improved. Then, a finite element model has been established for collaborative optimization, and a parameterized optimization scheme that meets the seismic reduction requirements has been obtained. The results show that the optimization method proposed in the study has a better effect in seeking the minimum cost, and meets the design requirements of the specification. The optimization scheme of prefabricated concrete frames designed by the research institute based on finite element analysis can efficiently optimize various parameters, greatly improving the structure energy dissipation and seismic performance.

Keywords: prefabricated concrete frame, energy dissipation and shock absorption, multi objective optimization, finite element analysis

[1]Associate Professor, MsC., Department of Civil and Architectural Engineering, Jiaozuo University, Jiaozuo, 454000, China, e-mail: jzulzj@163.com, ORCID: 0009-0005-5625-4880

1. Introduction

At present, research on prefabricated concrete frame (PCF) structural systems in China mainly focuses on the seismic performance analysis and design methods of PCF structural systems [1, 2]. Research has shown that PCF structures have advantages such as short construction cycles and reliable component connections, but their deformation and energy dissipation capabilities are poor under earthquake action, making them prone to damage and posing safety hazards [3,4]. To ensure the safety performance of the PCF structural system, it is necessary to carry out seismic control. Setting energy dissipation and shock absorption devices in a structure can reduce inter-story displacement angle under earthquake action, making the structure have good seismic performance without consuming too much manpower and material resources. Setting energy dissipation and shock absorption devices in PCF structures is a relatively economical and effective seismic absorption method. However, there is currently no unified standard for the optimization design of energy dissipation and shock absorption devices in PCF structures, and researchers can only propose corresponding optimization plans based on the actual engineering situation and theoretical calculation results [5]. Based on multi-objective optimization theory, parametric visualization modeling of structural model and finite element program, a parametric visualization optimization design flow is established. According to the characteristics of structures and nodes, a multi-objective optimization formula based on structural cost and damage energy ratio is proposed, and the optimization problem is analyzed. Finally, the prefabricated PC frame structure of the box is optimized by using the parametric visual structure optimization design tool, and the seismic cooperative optimization design based on different fortification levels is realized, and the dimensions and energy-consuming node parameters of the prefabricated components are optimized.

The article conducts research through four parts. The first part introduces current finite element analysis and energy dissipation and vibration reduction of prefabricated concrete frames. The second part is the design of PCF structure optimization scheme based on FEA. The third part is the performance verification of the research and design scheme. The fourth part is the conclusion.

2. Related works

Finite element analysis provides a more convenient and low-cost way to evaluate the concepts and details of design, which can evaluate the experimental process or replace physical experiments. It is widely used in many fields such as aviation, aerospace, civil engineering, machinery, water conservancy, materials, and so on. Yu et al. conducted finite element analysis to verify the effect of size effect coupling dynamic strain. They studied its influence on direct tensile strength of lightweight aggregate concrete as the research object to predict the dynamic direct tensile strength. As strain rate increased, the size effect weakened [6]. The Niu et al. proposed a method to reconstruct structural displacement, addressing the shortcomings of existing inverse finite element methods. The structure

displacement field was represented by scaling the boundary radially [7]. Saleh and other scholars established a concrete damage plastic model based on finite element analysis to study the mechanical characteristics of reinforced concrete deep beams with openings. They found that the increase of most parameters would lead to higher ultimate loads [8].

Due to the use of on-site assembly of finished products in the PCF structure, which has the advantages of high industrialization and short construction period, many researchers conducted relevant research on this topic. The Yin et al. formed a new prefabricated single-layer reinforced shear wall structure with steel tube concrete boundaries and reinforced concrete wall panels. In order to facilitate assembly and improve seismic resistance, the shear wall was connected to the main frame beam through high-strength bolts and subjected to lateral cyclic load tests. It was found that the deformation capacity of shear wall structures can satisfy elastic-plastic interlayer displacement ratio (1/100) in seismic design in practical engineering [9]. Scholars such as Li et al. proposed a prefabricated steel tube concrete frame node to fully leverage the advantages of steel tube concrete. Their seismic performance was studied through FEA, and it was found that the ductility coefficient was between 1.72 and 6.82, and the equivalent viscous damping coefficient was between 0.13 and 3.03, indicating a good energy dissipation capacity [10]. In order to improve buildings construction quality, Chen and Poongodi designed a new type of bolted connection method to connect prefabricated concrete frames. They studied its seismic resistance through related indicators. Results showed a good deformation capacity, with an energy dissipation coefficient of $E = 0.24$ [11].

In summary, although researchers have proposed many methods for seismic optimization of PCF structures and achieved certain results, with the increasing variety of numerical simulation analysis objects, the demand for FEA analysis efficiency and accuracy is also increasing. The research aims to improve the energy dissipation and seismic performance of PCF structures by introducing hysteresis curves and optimizing modeling parameters.

3. Design of PCF structure optimization scheme based on FEA

In this study, the existing finite element analysis is optimized to improve the engineering applicability of the analysis algorithm, so that the self-recovery and energy dissipation characteristics of the energy dissipation and damping nodes in the PCF structure can be simulated based on the improved finite element program. Then, the parametric structure of PCF energy dissipation and vibration reduction is optimized, and a collaborative optimization mathematical model is established to meet the structural requirements.

3.1. FEA optimization for PCF structures with dampers

Prefabricated structures are being widely promoted because of their advantages such as short construction period, small number of employees, small environmental impact and easy quality control. However, because the stiffness and strength of their joint connections are often lower than those of cast-in-place concrete joints, the integrity of the structures

is reduced, and the stiffness and strength are weakened [12, 13]. In this paper, a new type of post-tensioned prestressed prefabricated concrete frame beam-column joint energy dissipation and shock absorption joint is formed by using the damper applied to the beam-column joint. However, it has not been applied to the whole structure to study its seismic performance [14]. Therefore, it is necessary to study the prefabricated concrete frame with joint dampers based on seismic performance.

FEA software commands are mainly divided into three types, namely modeling, analysis, and output specification. The specific situation is shown in Fig. 1. Finite element analysis is performed by adding commands to the model. The continuous enrichment of functions of the finite element platform D-SAP provides convenience for the research of new structural systems. However, there are some deficiencies in materials, elements, and algorithms. Therefore, the research is carried out to supplement the functions of D-SAP for the research of prefabricated concrete frames containing node dampers. The hysteresis curve of the node is a "double flag", indicating that it has good self-recovery and energy consumption characteristics, and it is necessary to supplement the simulation material of this type of semi-rigid node in D-SAP.

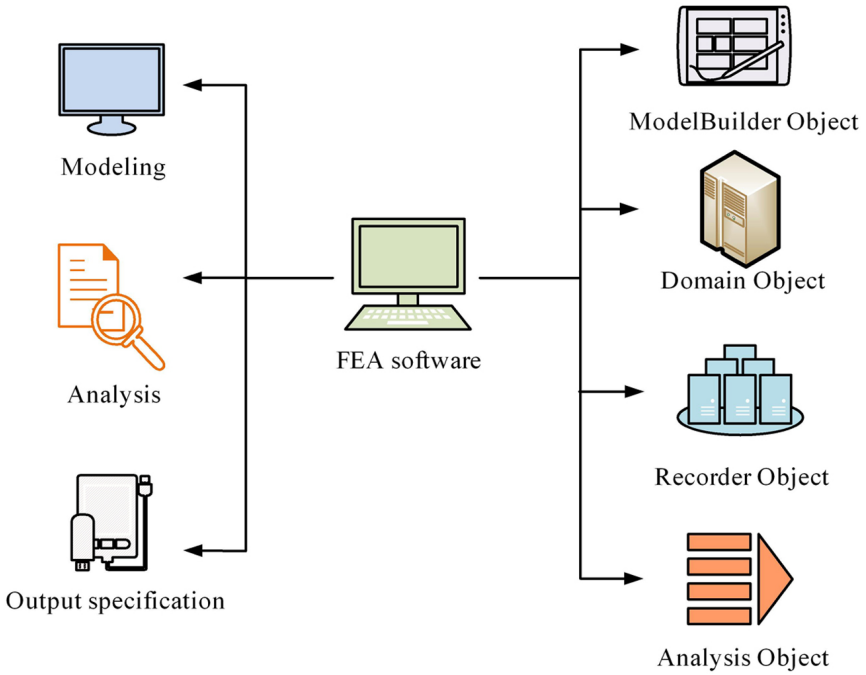

Fig. 1. Basic module of finite element analysis software

The hysteresis curve can generate the load-deformation relationship of structural components under repeated cyclic loads. It can determine the structural resilience model and conduct nonlinear seismic response analysis. To simulate material characteristics in finite element analysis, shape parameters of its hysteresis curve skeleton can be summarized

into 6, including: initial section stiffness coefficient K_1, reinforcement section stiffness coefficient K_2, unloading section stiffness coefficient K_2, yield bending moment value M_y, maximum strain value in the loading section θ_f, and energy dissipation coefficient β. The hysteresis rule has a strong correlation with the state parameters of the previous stage [15]. Therefore, when the stress state of each stage is corrected, the state parameters of each stage must be calculated in order to determine the stress state of the next stage.

Figure 1 is a schematic diagram of the stress state parameters of the material. Taking the first quadrant as an example, the stress state position corresponds to the coordinate position of the external inflection point of the hysteretic path with a slope of K_1 as (f_{OP}, F_{OP}), the coordinate position of the internal inflection point as (f_{IP}, F_{IP}) and the horizontal coordinate value of f_P intersecting the X-axis. The corresponding f_{IP}, F_{IP}, f_{OP}, F_{OP} and f_P are called the state parameters, similarly, the state parameters of the third quadrant are f_{IN}, F_{IN}, f_{ON}, F_{ON} and f_N. Where P and N represent the first and third quadrants. The hysteresis rule is closely related to a set of state parameters from the previous step.Therefore, these state parameters should be calculated at the same time when the stress state of the material is updated at each step to facilitate the determination of the stress state in the next step. According to the hysteresis curve of the material, the stiffness of the loading section and the unloading section of the hysteresis curve are inconsistent, indicating that the hysteresis circle is not a simple parallelogram, and the state parameters need to be derived to a certain extent. Fig. 2 takes the first quadrant as an example. According to geometric relationships, the horizontal distance between two points CD_1 can be represented by equation (3.1).

$$\frac{\left(\theta_f - \frac{M_y}{K_1}\right) K_2 (1-x)}{K_3} + \frac{\left(\theta_f - \frac{M_y}{K_1}\right) K_2}{K_1} x = \theta_f - \frac{M_y}{K_1} \tag{3.1}$$

In equation (3.1), x and $1 - x$ are the proportions of the two line segments and their total. According to equation (3.1), the horizontal direction calculation formula for DD_1 can be obtained, as shown in equation (3.2).

$$|DD_1| = \frac{\left(\theta_f - \frac{M_y}{K_1}\right) K_2}{K_1} x = \left(\theta_f - \frac{M_y}{K_1}\right) \frac{K_2 - K_3}{K_1 - K_3} \tag{3.2}$$

The horizontal spacing of DD_1 is the product of the spacing between AB or CD_1 points and a certain stiffness correlation coefficient. There is a proportional relationship between the horizontal distance between any loading and unloading path P with a stiffness coefficient of K_1 and the intersection point EE_1 of the actual unloading curve and the assumed unloading curve, and the horizontal distance between two points DD_1, as shown in equation (3.3).

$$|EE_1| = k \left(\theta_f - \frac{M_y}{K_1}\right) \frac{K_2 - K_3}{K_1 - K_3} \tag{3.3}$$

The horizontal distance between the two points of CE_1 can be expressed as $k\left(\theta_f - M_y/K_1\right)$ by the triangle analogy in equation (3.4). So, the horizontal distance between two points of

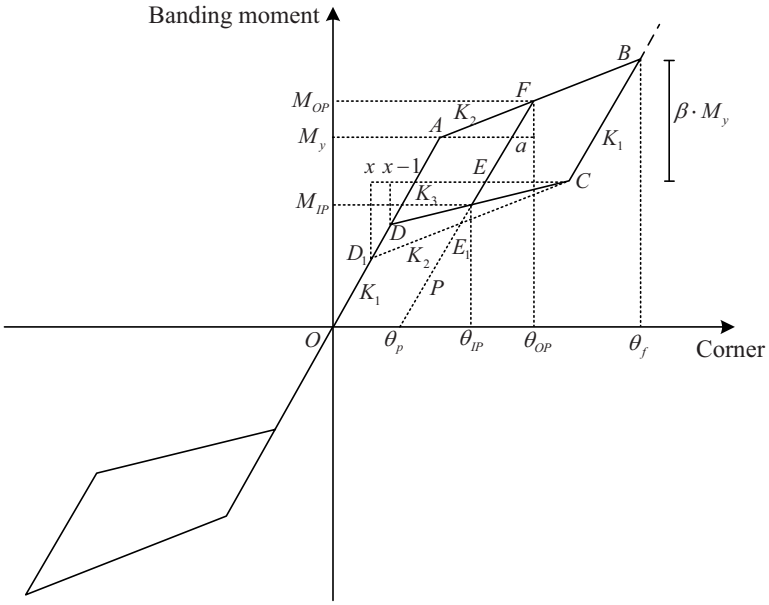

Fig. 2. Material stress state parameters

EE_1 and the horizontal distance between two points of CE_1 are also proportional, and its proportional coefficient is called the solving coefficient of the state parameter, represented by α, and its expression is equation (3.4).

$$\alpha = \frac{K_2 - K_3}{K_1 - K_3} \tag{3.4}$$

The material strain value is represented as T_{strain} and the stress value as T_{stress}. If θ_{OP} is less than T_{strain}, the current strain and stress values, i.e. the coordinates of the outer inflection point, are (θ_{OP}, M_{OP}).

If θ_{IP} is greater than T_{strain}, the coordinates of the inner inflection point are expressed as (θ_{IP}, M_{IP}). Based on the geometric relationship, $\theta_P = \theta_{IP} - \frac{M_{IP}}{K_1}$ and $\frac{K_1 a}{K_2} = \theta_P + a$ can be obtained according to the geometric relationship.

Because the coordinates of the outer inflection point are only proportional to θ_p, the proportional coefficient γ between them is called the solving coefficient of the state parameter, and its mathematical expression is equation (3.5).

$$\gamma = \frac{K_1}{K_1 - K_2} \tag{3.5}$$

The difference in stiffness between the loading and unloading sections is reflected in the hysteresis curve, which is manifested as the difference in curve slope. If the difference between the two is too large or the value of β is too small, it will cause the two parts of

the loading and unloading sections to intersect geometrically. In order to avoid the above situation, an inequality as shown in equation (3.6) was constructed.

$$\beta \geq \left(\frac{\theta_f K_1}{M_y} - 1\right) \frac{K_2 - K_3}{K_1 - K_3} \tag{3.6}$$

For the analysis function of FEA for prefabricated structures, there is a lack of simulation materials for beam column semi rigid joints with "double flag" hysteresis performance. Therefore, the study utilizes the modular structure of FEA software itself to add a new uniaxial material to the material library, which can be used to write programs that implement the material's functions. Other modules only need to be supplemented and improved as needed.

3.2. Parameterized structural optimization design of energy dissipation and vibration reduction for PCF

To improve the efficiency of PCF optimization, based on the improvement of the FEA program's analysis and simulation function for PCF structures, the optimization design of the energy dissipation and vibration reduction parameterized structure of PCF structures was carried out. Under earthquake action, the seismic performance optimization design of structures should defend not only small earthquakes, but also large earthquakes. For the sake of convenience, some researchers have used a two-stage optimization method based on reasonable assumptions for the optimal solution of such problems [16–18]. However, the two-stage optimization scheme cannot simultaneously meet the seismic requirements of both small and large earthquakes. Therefore, the study does not use two-stage optimization, but instead uses collaborative optimization of small and large earthquakes. The study first optimized the structural cost. With basic composition of prestressed PCF structures, calculation formula for total cost f_1 of the structure can be expressed as equation (3.7).

$$\begin{cases} f_1 = P_1 + P_2 + P_3 \\ P_1 = p_c \sum_{1}^{N} v_{ci} \\ P_2 = \sum_{1}^{N} v_{pi} p_{pi} \\ P_3 = P_d + P_{d3} \end{cases} \tag{3.7}$$

In equation (3.7), P_1 represents the cost of the frame prefabricated component, P_2 represents the cost of prestressed steel strands, P_3 represents the cost of dampers, p_c represents the current market unit price of prefabricated prefabricated components, v_{ci} represents the amount of prefabricated components in the i layer, N counts frames, v_{pi} represents the amount of prestressed steel strands in the i layer, p_{pi} represents the unit price of prestressed steel strands in the i layer. Due to the integrated anchoring steel plates and ear plates, During the design process, the specifications do not change, and the pins and high-strength bolts are priced based on the number of pieces and the unit price is relatively small, almost unaffected by design variables. Therefore, this part is represented

by the constant P_d, where P_{d3} represents the sum of the cost of the damper steel plate and transmission rod steel plate, which can be expressed as equation (3.8).

$$P_{d3} = p_d \sum_{1}^{N} m_{di} c_{di} \tag{3.8}$$

In equation (3.8), p_d represents the market unit price of the steel plate considered for processing, m_{di} represents the number of dampers in layer i, and c_{di} represents the sum of the amounts of friction damper steel plate and transmission rod steel plate used in a single damper in layer i.

The performance requirements of the whole layer of the structure mainly focus on the strength, stiffness and stability of the whole structure, including the displacement Angle between the layers, shear weight ratio and rigid weight ratio. The main purpose of limiting the inter story displacement angle index in structural design is to limit the horizontal structure displacement, ensure high-rise structure stiffness, prevent excessive deformation, and thus affect the structure bearing capacity, stability, and usage requirements. The inter story displacement angle requirements are shown in equation (3.9).

$$\begin{cases} \mathrm{SDE}(i) \le [\mathrm{SDE}] \\ \mathrm{SDP}(i) \le [\mathrm{SDP}] \end{cases} \tag{3.9}$$

In equation (3.9), $\mathrm{SDE}(i)$ represents the elastic interlayer displacement angle of the i layer, $\mathrm{SDE}(i)$ represents the elastic-plastic angle of the i layer, $[SDE]$ represents the structural elastic angle limit specified in the specification, and [SDP] represents the structural elastic-plastic angle limit specified in the specification. In seismic checking calculation, the purpose of weight loss ratio index is mainly to control the minimum seismic shear force of each floor and ensure the safety of the structure. The horizontal seismic shear force of any floor of the structure shall conform to $V_{\mathrm{EK}}(i) \ge \lambda \sum_{j=1}^{N} G_j$. The stiffness to weight ratio is the main parameter affecting the second-order effect of gravity. High rise frame structures should comply with $D_i \ge 10 \sum_{j=1}^{n} G_j / h_i$. D_i and h_i respectively represent the stiffness to weight ratio and height of the i layer, and G_j represent gravity load representative value of j layer.

The design requirements of component level constraint mainly focus on component size and ductility. The size range of the frame column can be set according to the "Code for Seismic Design of Buildings" GB 50011-2010 (2016 edition). In order to control the ductility of the column, limit the axial compression ratio of the column by $[\mu_N] = \dfrac{N}{f_c A_c}$.

At the beam-column joint surface of an unbonded prestressed fully assembled concrete frame, the ratio of the ultimate flexural capacity M_{su} of the energy-consuming steel bar to the ultimate flexural capacity M_u of the section should meet $0.3 \le \dfrac{M_{su}}{M_u} \le 0.5$.

4. Parameterized structural optimization results analysis for energy dissipation and vibration reduction

The study provides a brief overview of the performance testing process and results. It employs large-scale universal FEA to simulate PCF structure and then compares it with test results to validate the reliability of the finite element model. With the model established, a comprehensive analysis of the structure's seismic performance is conducted to gain deeper insights.

4.1. Parameter optimization results analysis

In order to ensure the optimization efficiency, it is assumed that each type of optimization object has the same value in the three layers, and the optimization parameters of this structure are 4 types and 16. The height of the design columns is 3.6 m. The beam span length is 6 m, located in an area with a fortification intensity of 8 degrees (0.20 g), the site category is Class II, the design seismic group is Group II, and the site characteristic period value is 0.40 s. Other parameters are shown in Table 1.

Table 1. Parameter details table

Materials	Design value of tensile strength	Modulus of elasticity	Argument	Index
C40 Concrete	19.1 N/mm^2	3.25×10^4 N/mm^2	Height of column	3.6 m
HRB400 rebar	360 N/mm^2	2.00×10^5 N/mm^2	Beam span	6 m
HPB300 prestressed tendons	270 N/mm^2	1.95×10^{11} N/mm^2	Design upper limit of yield bending moment	500 kN· m
The damper is made of Q420 steel	420 N/mm^2	3.25×10^4 N/mm^2	Design upper limit of joint yield Angle	20×10^{-3} rad

The study conducted 5 calculations using the same parameters to ensure the quality of parameter optimization. Fig. 3(a) shows the distribution of the final Pareto solution set for the five instances that have been calculated, using the first Pareto solution set of one instance as a reference. Fig. 3(b) shows the distribution of feasible regions and the final Pareto solution set for the feasible solution of calculation example 1.

Through comparison, it can be seen that after 300 iterations, the Pareto front effectively moves towards a more optimized direction compared to the first generation, and has high consistency in distribution. This proves that the improved optimization algorithm proposed by the research institute is reliable in solving this problem. Among them, compared with other cases, the Pareto solution set of Case 1 has a more dispersed distribution on the frontier

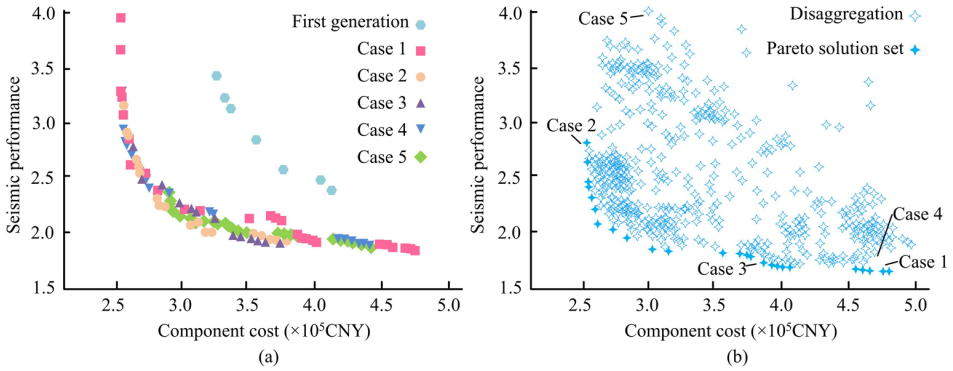

Fig. 3. Effect analysis of Pareto solution set: a) Pareto solution set, b) Distribution of feasible solutions for Case 1

and its quality is much better than other cases. Therefore, it is selected as the discussion object for verifying the optimization results in the following text.

Five feasible solutions for relatively special locations were selected to verify the optimization results: Individual Case 1 with the best seismic performance index, individual Case 2 with the lowest structural scheme cost, individual Case 3 with the best seismic performance index of the initial generation and individual Case 5 with the lowest structural scheme cost were selected respectively. Table 2 lists the cost and energy dissipation seismic performance details of these 5 cases, from which it can be seen that the structural cost is mainly controlled by prefabricated components; The cost of Example 2 decreased by 15.91% compared to Example 5, indicating that the optimization method proposed in the study has better effectiveness in seeking the minimum cost; Although no significant difference showed between Case 1 and Case 4, the seismic response of Case 2 has decreased by 35.08% compared to Case 4.

Table 2. Case individual target values

Case	Structural cost (105 CNY)	Structural cost component (105 CNY)				Seismic performance index
		Steel strand	Damper	Precast beam	Precast column	
1	4.821	0.163	0.104	2.276	2.293	1.803
2	2.609	0.108	0.076	1.612	1.256	3.826
3	3.736	0.126	0.076	1.746	1.794	2.083
4	4.625	0.156	0.076	2.091	2.293	1.885
5	3.093	0.179	0.089	1.486	1.322	5.873

4.2. Analysis of energy dissipation and shock absorption performance

Figure 4 shows the vertical distribution of some parameters in the PCF structure. From Case 1 and Case 4 in Fig. 4(a), it can be found that there is a certain correlation between increasing the initial pre tension of prestressed steel strands as evenly as possible along the floor and improving the seismic performance of the structure. From Case 1 to 3, the average level of initial pre tension of prestressed steel strands is inversely proportional to their seismic performance. In Fig. 4(b), in the structural scheme, the pre tightening force of all dampers and high-strength bolts is at the minimum level, which is 100 kN, indicating that the structural scheme is feasible. As shown in Fig. 4(c), the upper part is reduced earlier than the lower part, and it can be considered that the size of the lower column has a greater impact on structure seismic performance than the upper part. The total structure weight in Fig. 4(d) is directly proportional to the degree of excellence in energy dissipation and shock absorption performance.

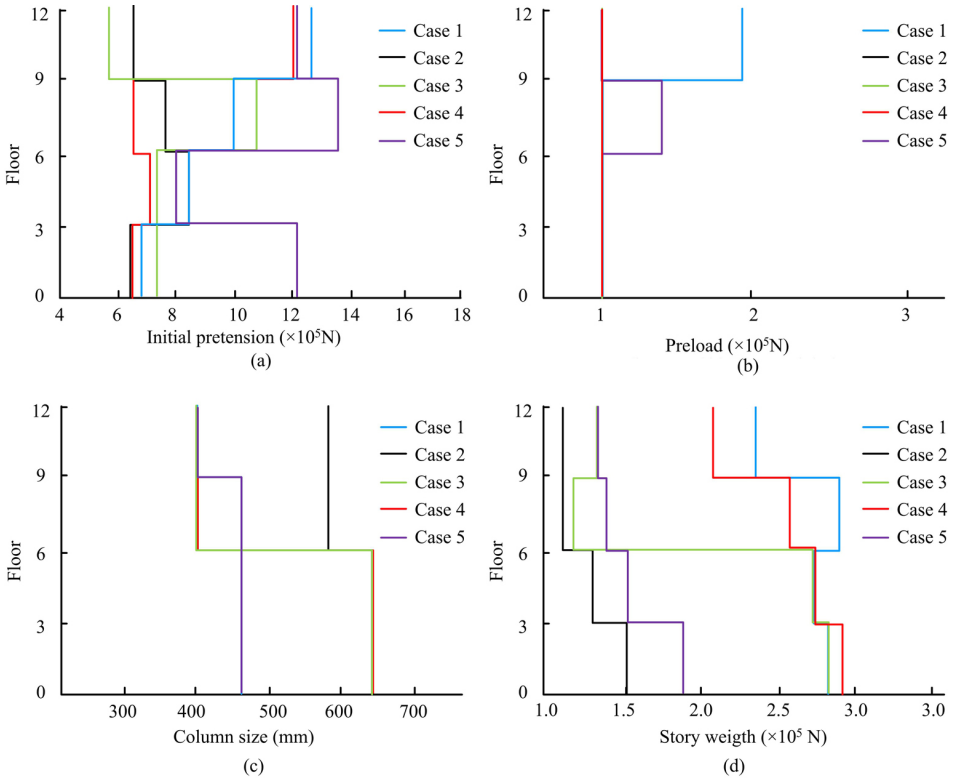

Fig. 4. Vertical distribution of structural parameters: a) Influence of prestressed strand on seismic performance, b) Influence of high strength bolts on seismic performance, c) Influence of prefabricated columns on seismic performance, d) Effect of layer weight on seismic performance

The study provides the vertical distribution of several main performance indices of concrete fibers. Figs. 5(a) and 5(b) show the maximum interlayer displacement angle distribution of each case. The results indicate that the vertical distribution maps of each case under the action of small earthquakes are relatively concentrated, significantly less than the 1/550 specified in the specifications. However, in the event of a major earthquake, individuals are still relatively dispersed, especially in cases 1, 3, and 4 with excellent seismic performance, which are much larger than cases 2 and 5 with cost advantages. The better the seismic performance, the greater the maximum angle.

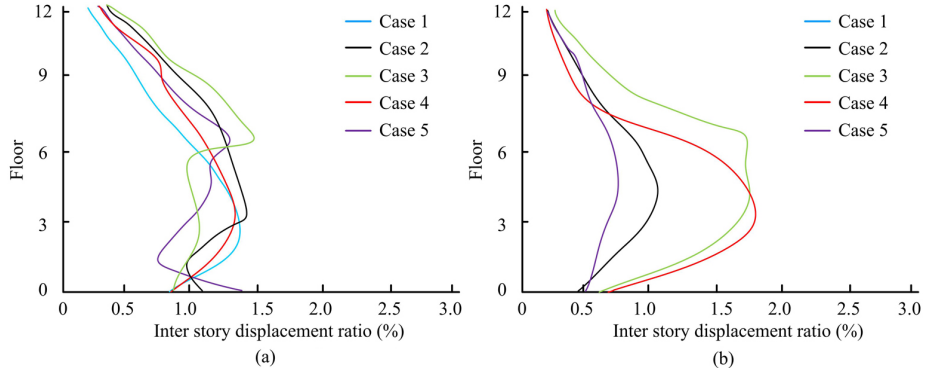

Fig. 5. Vertical comparison of structural properties: a) Small earthquake level, b) Magnitude of major earthquake

The distribution of left and right tower structures angles under rare earthquakes is shown in Fig. 6. The maximum PCF structure lateral angle under rare earthquakes is 1/168, and the maximum vertical angle is 1/193. The maximum angle in both directions did not exceed 0.009, meeting the specified design requirements.

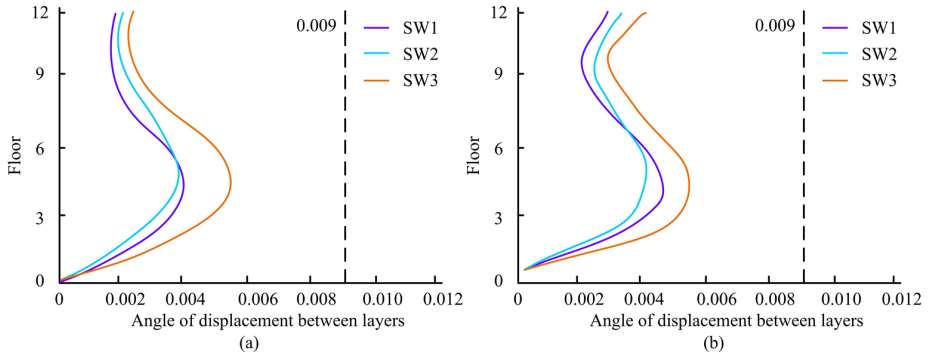

Fig. 6. Analysis of displacement angle between layers: a) Lateral interlayer displacement angle comparison, b) Comparison of displacement angle between vertical layers

The comparison between the base shear force calculated from the 7 seismic wave time history curves and the base shear force obtained from the mode decomposition response spectrum method in the elastic time history analysis of frequent earthquakes is shown in

Table 3. From the table, the base shear force obtained from time history analysis is 65% more and 135% less than that obtained from response spectrum method. The average force is greater than 80% of the response spectrum method and less than 120% of the response spectrum method, indicating that the obtained seismic waves can meet engineering design and analysis requirements.

Table 3. Comparison between elastic time history analysis and response spectrum base shear force

Seismic wave	Landscape orientation		Vertical	
	Base shear (kN)	Ratio (%)	Base shear (kN)	Ratio (%)
Response spectrum method	4671.2	–	4596.2	–
1	4372.6	93.62	4632.9	100.94
2	4277.3	91.52	4513.6	98.45
3	4228.64	103.46	4251.9	92.14
4	3923.3	90.23	3701.8	80.14
5	4957.7	86.39	3664.2	79.35
6	4784.6	106.57	4358.1	94.52
7	4837.9	102.33	5400.3	117.39
Time-history average	4506.66	96.30	4389.88	94.70

5. Conclusions

In order to ensure the safety and reliability of precast concrete frame under different fortify grade, hysteresis curve is introduced in finite element analysis, mathematical model based on cooperative optimization is established, and parametric energy dissipation and shock absorption optimization of polyvinyl chloride fiber structure is completed. The results showed that the cost of PCF structure was mainly controlled by prefabricated components, and the cost of Case 2 was reduced by 15.91% compared to Case 5, indicating that the optimization method proposed in the study had better effectiveness in seeking the minimum cost. Case 2 had a 35.08% decrease in energy dissipation and seismic performance compared to Case 4. The load and displacement were both within 10%, while the maximum deviation between yield load and ultimate load was within 3%. The maximum interlayer displacement angle of each case under small and large earthquakes was significantly less than the 1/550 specified in the code. The maximum lateral interlayer displacement angle of PCF structure under rare earthquake action was 1/168, and the maximum vertical interlayer displacement

angle was 1/193, meeting the design requirements of the code. The research based on finite element analysis improves the efficiency of parametric optimization of precast concrete frame structure, and enhances the energy dissipation and seismic performance of precast concrete frame structure. However, when the height of the structure is further increased or the structure is transformed into a three-dimensional form, the optimized spatial scale will increase exponentially, and the elastic-plastic analysis time will also increase significantly. How to optimize the structure elastoplastic in a limited time is still a problem to be solved in the future.

References

[1] J. Dong, H. Liu, S. Xia, Y. Cheng, M. Lei, and Z. Chen, "Experimental research and finite element analysis on structural stability of disc-buckle type formwork Support", *International Journal of Steel Structures*, vol. 22, no. 3, pp. 748–746, 2022, doi: 10.1007/s13296-022-00603-4.

[2] A.M. Usman, and M.K. Abdullah, "An assessment of building energy consumption characteristics using analytical energy and carbon footprint assessment model", *Green and Low-Carbon Economy*, vol. 1, no. 1, pp. 28–40, 2023, doi: 10.47852/bonviewGLCE3202545.

[3] L. Li, Z. Wei, D. Zhang, J. Wang, and X. Shi, "Finite element analysis of the effects of load amplitude and phase on crack initiation location in fretting fatigue", *Proceedings of the Institution of Mechanical Engineers, Part C. Journal of Mechanical Engineering Science*, vol. 235, no. 23, pp. 7091–7100, 2021.

[4] V.D. Gazman, " A new criterion for the ESG model", *Green and Low-Carbon Economy*, vol. 1, no. 1, pp. 22–27, 2023, doi: 10.47852/bonviewGLCE3202511.

[5] A. Islam, F. Othman, N. Sakib, and H. Babu, "Prevention of shoulder-surfing attack using shifting condition with the digraph substitution rules", *Artificial Intelligence and Applications*, vol. 1, no. 1, pp. 58–68, 2023, doi: 10.47852/bonviewAIA2202289.

[6] W. Yu, L. Jin, X. Liu, and X.L. Du, "Mesoscopic finite element analysis on dynamic direct tensile failure of lightweight aggregate concrete and corresponding size effect", *International Journal of Damage Mechanics*, vol. 31, no. 3, pp. 403–425, 2022, doi: 10.1177/10567895211044189.

[7] S. Niu, Y. Zhao, and H. Bao, "Shape sensing of plate structures through coupling inverse finite element method and scaled boundary element analysis", *Measurement*, vol. 190, no. 28, 2022, doi: 10.1016/j.measurement.2021.110676.

[8] M. Saleh, M. Alhamaydeh, and M. Zakaria, "Finite element analysis of reinforced concrete deep beams with square web openings using damage plasticity model", *Engineering Structures*, vol. 278, no. 15, pp. 221–257, 2023, doi: 10.1016/j.engstruct.2022.115496.

[9] F. Yin, W.L. Cao, R.W. Wang, H.F. Weng, and Y.B. Liu, "Seismic behavior of prefabricated concrete filled steel tube-bordered monolayer reinforced shear wall", *Journal of Constructional Steel Research*, vol. 194, no. 6, pp. 67–83, 2022, doi: 10.1016/j.jcsr.2022.107328.

[10] S. Li, D. Zhao, and Y. Zhou, "Research on seismic performance of prefabricated concrete-filled steel tubular frame joints", *International Journal of Structural Integrity*, vol. 13, no. 2, pp. 327–347, 2022, doi: 10.1108/IJSI-08-2021-0087.

[11] S. Chen and M. Poongodi, "An exhaustive research and analysis on seismic performance of prefabricated concrete shear wall structure", *Journal of Vibroengineering*, vol. 22, no. 8, pp. 1871–1883, 2020, doi: 10.21595/jve.2020.21628.

[12] K. Jain and A. Saxena, "Simulation on supplier side bidding strategy at day-ahead electricity market using ant lion optimizer", *Journal of Computational and Cognitive Engineering*, vol. 2, no. 1, pp. 17–27, 2023, doi: 10.47852/bonviewJCCE2202160.

[13] Y. Huang, "On the resistance of concrete hollow thin-walled high piers to rock collisions", *Archives of Civil Engineering,* vol. 69, no. 3, pp. 187–197, 2023, doi: 10.24425/ace.2023.146075.

[14] G. Muhiuddin, A. Mahboob, and M.E.A. Elnair, "A new study based on fuzzy bi-Γ-ideals in ordered-Γ-semigroups", *Journal of Computational and Cognitive Engineering*, vol. 1, no. 1, pp. 42–46, 2022, doi: 10.47852/bonviewJCCE19919205514.

[15] Y. Yang and X. Song, "Research on face intelligent perception technology integrating deep learning under different illumination intensities", *Journal of Computational and Cognitive Engineering*, vol. 1, no. 1, pp. 32–36, 2022, doi: 10.47852/bonviewJCCE19919.

[16] S. Choudhuri, S. Adeniye, and A. Sen, "Distribution alignment using complement entropy objective and adaptive consensus-based label refinement for partial domain adaptation", *Artificial Intelligence and Applications*, vol. 1, no. 1, pp. 43–51, 2023, doi: 10.47852/bonviewAIA2202524.

[17] X.M. Long, Y.J. Chen, and J. Zhou, "Development of ar experiment on electric-thermal effect by open framework with simulation-based asset and user-defined input", *Artificial Intelligence and Applications*, vol. 1, no. 1, pp. 52–57, 2023, doi: 10.47852/bonviewAIA2202359.

[18] Y.X. Jin, M. Xu, and J. Jia, "Analysis of the seismic performances of structures reinforced by self-centering buckling-restrained braces", *Archives of Civil Engineering,* vol. 69, no. 3, pp. 645–663, 2023, doi: 10.24425/ace.2023.146103.

Received: 2023-09-28, Revised: 2023-12-16